Neutron Scattering Study of the Structural Change Induced by Photopolymerization of AOT/D(2)O/Dodecyl Acrylate Inverse Microemulsions

ARTICLE *in* LANGMUIR · NOVEMBER 2008

Impact Factor: 4.46 · DOI: 10.1021/la8022634 · Source: PubMed

3 AUTHORS, INCLUDING:

Jolanta E. Marszalek
University of Akron
6 PUBLICATIONS **53** CITATIONS
SEE PROFILE

John Pojman
Louisiana State University
238 PUBLICATIONS **4,139** CITATIONS
SEE PROFILE

Langmuir

Article

Neutron Scattering Study of the Structural Change Induced by Photopolymerization of AOT/DO/Dodecyl Acrylate Inverse Microemulsions

Jolanta Marszalek, and John A. PojmanKirt A. Page

Langmuir, **2008**, 24 (23), 13694-13700 • Publication Date (Web): 04 November 2008

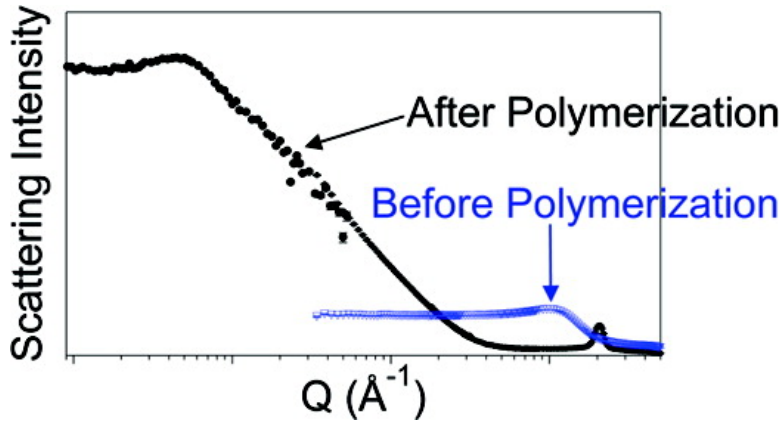

More About This Article

Additional resources and features associated with this article are available within the HTML version:

- Supporting Information
- Access to high resolution figures
- Links to articles and content related to this article
- Copyright permission to reproduce figures and/or text from this article

View the Full Text HTML

Neutron Scattering Study of the Structural Change Induced by Photopolymerization of AOT/D_2O/Dodecyl Acrylate Inverse Microemulsions

Jolanta Marszalek and John A. Pojman*,†

Department of Chemistry and Biochemistry, The University of Southern Mississippi, Hattiesburg, Mississippi 39406-0001

Kirt A. Page*

National Institute of Standards and Technology, Materials Science and Engineering Laboratory, Polymers Division, Gaithersburg, Maryland 20899-8540

Received July 15, 2008. Revised Manuscript Received September 16, 2008

Small-angle and ultrasmall-angle neutron scattering (SANS/USANS) measurements were used to determine the structural changes induced by photopolymerization of AOT/D_2O/(dodecyl acrylate) inverse microemulsion systems. Scattering profiles were collected for the initial microemulsions and the films resulting from photopolymerization of the oil phase. The SANS data for the microemulsions were modeled as spherical, core−shell droplets. Upon polymerization, the clear mircoemulsions formed opaque films. From the SANS/USANS data of the films, it was apparent that this morphology was not preserved upon polymerization; however, it was clearly observed that the formulation of the microemulsion had a large impact on the structure within the films. The Guinier region in the USANS data (2.5×10^{-5} Å$^{-1} \leq Q \leq 5.3 \times 10^{-3}$ Å^{-1}) from the films indicates that very large structures are formed. Simultaneously, a well-defined peak (0.15 Å$^{-1} \leq Q \leq 0.25$ Å^{-1}) in the SANS data indicates that there are also much smaller structures formed. It is proposed that the low-Q scattering arises from aggregation of the nanometer-size water droplets in the microemulsion to form droplets large enough to scatter visible light, while the peak in the high-Q region results from bilayered structures formed by the surfactant.

Introduction

Microemulsions are thermodynamically stable mixtures of oil and water, where the water−oil interface is stabilized by the presence of a surfactant. The microstructure of a microemulsion depends on the composition of the system, temperature, and pressure. Water in oil (w/o) droplets form at lower water content, and the opposite is true for lower oil content. Microemulsion systems display a rich phase behavior[1−7] that can include morphologies as varied as spherical droplets, "sponge" phases,[8] and lamellar phases,[9] all of which can have structure on the nanometer scale. In particular, typical water-in-oil microemulsions are characterized by the existence of nanometer-sized water droplets stabilized by surfactant (i.e., inverse micelles) that are dispersed in a continuous phase of oil.[10,11] Stable, spontaneous droplet formation is facilitated by the ability of the surfactant to effectively bridge the two immiscible fluids, by sufficiently reducing the interfacial surface tension between the oil and water phases, resulting in the formation of macroscopically homogeneous but microscopically heterogeneous systems.[12,13] Due to the nanometer size of the water domains, these systems are optically transparent.

The use of microemulsion structure as a template for the synthesis of polymeric materials has received a considerable amount of attention.[14−16] Typically, microemulsion polymerizations are used in the synthesis of well-defined, nanometer-sized polymer particles with a narrow size distribution. Although a full discussion of this topic is beyond the scope of this paper, it can be stated that the inherent properties of microemulsion systems give a large degree of control over the polymerization process and, ultimately, the types of polymer particles that can be synthesized.[14] Specifically, inverse-microemulsion polymerization is an attractive approach for the synthesis of high-molecular-weight water-soluble polymers[14,17] as well as difficult to dissolve polymers[18] such a polyaniline[19] or polythiophene.[20] It has also been shown that, in the restricted environment of inverse micelles, water exhibits unique physical and chemical

* To whom correspondence should be addressed. E-mail: kirt.page@nist.gov (K.A.P.); john@pojman.com (J.A.P.).

† Current Address: Department of Chemistry, Louisiana State University, Baton Rouge, LA 70803-1804.

(1) Eastoe, J.; Nave, S.; Penfold, J. *Langmuir* **2000**, *16*(23), 8733–8740.
(2) Saito, H.; Shinoda, K. *J. Colloid Interface Sci.* **1968**, *26*(1), 70–74.
(3) Harada, M.; Shioi, A.; Matsumoto, K. *J. Phys. Chem.* **1991**, *95*, 7495–7502.
(4) Eicke, H.-F.; Borkovec, M.; Das-Gupta, B. *J. Phys. Chem.* **1989**, *93*(1), 314–317.
(5) Kunieda, H.; Shinoda, K. *J. Colloid Interface Sci.* **1979**, *70*(3), 577–583.
(6) Moulik, S. P.; Paul, B. K. *Adv. Colloid Interface Sci.* **1998**, *78*, 99–195.
(7) Hellweg, T. *Curr. Opin. Colloid Interface Sci.* **2002**, *7*, 50–56.
(8) Javierre, I.; Nallet, F.; Bellocq, A.-M.; Maugey, M. *J. Phys.: Condens. Matter* **2000**, *12*, A295–A299.
(9) Nagao, M.; Okabe, S.; Shibayama, M. *J. Chem. Phys.* **2005**, *123*, 144909-1–8.
(10) Eastoe, J.; Robinson, B. H.; Steytler, D. C.; Thorn-Leeson, D. *Adv. Colloid Interface Sci.* **1991**, *36*, 1–31.
(11) Robinson, B. H.; McDonald, J. A.; Dore, J. C.; North, A. N.; Heenen, R. K.; Howe, A. M. *Colloids Surf.* **1986**, *19*, 21–29.
(12) Texter, J. *Colloids Surf., A* **2000**, *167*, 115–122.
(13) Miller, C. A.; Nishimi, T. *Langmuir* **2000**, *16*, 9233–9241.
(14) Hentze, H.-P.; Kaler, E. W. *Curr. Opin. Colloid Interface Sci.* **2003**, *8*(2), 164–178.
(15) Gan, L. M.; Li, T. D.; Chew, C. H.; Teo, W. K.; Gan, L. H. *Langmuir* **1996**, *12*, 5863–5868.
(16) Kaler, E. W.; de Vries, R.; Co, C. C. *Macromolecules* **2001**, *34*, 3224–3232.
(17) Li, X.; Xia, S. P.; Zeng, W. J.; Zhang, W. Y.; Dong, S. X. *Chin. Chem. Lett.* **2006**, *17*(2), 247–250.
(18) Jang, J. *Adv. Polym. Sci.* **2006**, *199*, 189–259.
(19) Yan, F.; Xue, G. *J. Mater. Chem.* **1999**, *9*, 3035.
(20) Tasakova, V.; Winkels, S.; Schultze, J. W. *Electrochim. Acta* **2000**, *46*, 759.

10.1021/la8022634 CCC: $40.75
Published on Web 11/04/2008

properties and facilitates the synthesis of various types of colloidal particles of inorganic solids (e.g., metals, metal carbonates, semiconductors).[21,22]

Although there have been several studies demonstrating the ability of carrying out polymerization reactions *within* the micelles of a microemulsion,[20,23] there has been little work on polymerizations that occur throughout the continuous phase of the microemulsion.[24−26] These works were concerned with polymerization of a monomer in a bicontinuous microemulsion to form porous polymers to be utilized as membranes.[27] Because the resulting polymers often did not reflect the original microstructure, polymerizable surfactants were introduced.[28,29] In another attempt to preserve the lamellar nanostructure of the microemulsion, a small amount of cross-linking throughout the oil phase resulted in nanostructured polyacrylamide hydrogels.[30] Here, we present work on the photopolymerization of the oil phase of the reverse microemulsion.

In a recent work,[31] Marszalek et al. demonstrated the ability to form films composed of a hydrophobic polymer matrix with an aqueous phase distributed throughout. Clear microemulsions of monomers, surfactant, and water were photopolymerized into opaque materials. The initially clear state of the w/o microemulsion indicates that the aqueous component is dispersed on the nanometer length scale. After photopolymerization, the opacity of the films indicates that aggregation of the aqueous phase leads to structures whose size exceeds the wavelength of visible light, namely, 500 nm.

As mentioned above, microemulsion systems display a rich phase behavior; therefore, the use of a polymerizable oil phase in inverse microemulsion systems provides an opportunity to create well-designed, nanostructured, polymeric materials for a variety of potential applications (functional membranes, separation membranes, fuel cells, etc.). By controlling the formulation of the microemulsion, one has a large degree of control over the size and shape of the resulting phase structures, which is likely to have a large impact on the relevant physical properties (i.e., transport) for a given application. It is, therefore, crucial to develop a fundamental understanding of the relationship between the "solution" microemulsion structure and the resulting structure in the polymerized microemulsion film. By understanding this structural relationship, it should be possible to rationally design high-performance, nanostructured films for targeted applications. We have chosen to address this interesting problem through the use of small-angle and ultrasmall-angle neutron scattering (SANS/USANS). Herein, we present analysis of SANS and USANS data for a series of microemulsions that reveal a significant change in structure upon polymerization. On the basis of the analysis of these data, we propose a model to describe the scattering behavior for these materials.

(21) Kawai, T.; Usui, Y.; Kon-No, K. *Colloids Surf., A* **1999**, *149*, 39.
(22) Chen, Z.; Li, S.; Yan, Y. *Chem. Mater.* **2005**, *17*, 2262–2266.
(23) Tang, R.; Xue, Y.; Yang, W.; Zha, L.; Fu, S. *J. Macromol. Sci., Part A: Pure Appl. Chem.* **2007**, *44*(6), 569–575.
(24) Cheung, H. M.; Sasthav, M.; Palani Raj, W. R. *Polymer* **1995**, *36*(13), 2637.
(25) Zhang, G.; Xu, X.; Tang, J.; Liu, H.; Ge, H.; Zeng, Z. *J. Appl. Polym. Sci.* **2000**, *77*, 1989–1993.
(26) Cheung, H. M.; Sasthav, M. *Langmuir* **1991**, *7*, 1378.
(27) Texter, J.; Yan, F. *Angew. Chem.* **2007**, *46*, 2440–2443.
(28) Texter, J.; Ge, L.; Mourey, T. H.; Bryan, T. G. *Langmuir* **2004**, *20*, 11288–11292.
(29) Tieke, B.; Pyckhout-Hintzen, W.; Dreja, M. *Macromolecules* **1998**, *31*, 272–280.
(30) Guymon, C. A.; Lester, C. L.; Smith, S. M. D. C. C. *Chem. Mater.* **2003**, *15*, 3376–3384.
(31) Marszalek, J.; Pojman, J. A.; Aultman, K. L.; Hoyle, C.; Whitehead, J. B. *J. Appl. Polym. Sci.* **2007**, *106*, 1957–1963.

Table 1. Parameters for the Microemulsion Formulations Used in This Study

$\phi_{w/s}$	W = [D2O]/[AOT]	monomers ϕ_m	AOT ϕ_s	D_2O ϕ_w
0.23	4.9	0.67	0.27	0.07
0.26	5.7	0.44	0.44	0.12
0.44	9.4	0.88	0.086	0.037
0.45	9.7	0.78	0.15	0.069
0.48	10.3	0.69	0.21	0.099
0.50	10.7	0.62	0.25	0.13
0.53	11.3	0.56	0.29	0.15
0.56	12.0	0.51	0.31	0.18
0.59	12.8	0.81	0.12	0.072
0.69	14.8	0.60	0.24	0.16

Experimental Methods

Materials. The dioctyl sulfosuccinate sodium salt (AOT) surfactant (>96% purity) and the deuterium oxide, D_2O (99.9 6 atom % D), were purchased from Aldrich. The monomer, dodecyl acrylate (DDA) at 90% purity was purchased from Sartomer, the cross-linker hexanediol diacrylate (HDDA) with >99% purity was purchased from Cytec Surface Specialties, and the photoinitiator Irgacure 369 was purchased from Ciba Specialty Chemicals. All materials were used as received. (Certain equipment, instruments, or materials are identified in this paper in order to adequately specify experimental details. Such identification does not imply recommendation by the National Institute of Standards and Technology nor does it imply the materials are necessarily the best available for the purpose.)

Preparation of Microemulsions. All microemulsions were prepared according the following procedure: A stock solution of a 5.7 mass fraction (%) mixture of the HDDA cross-linker with the respect to the DDA monomer was prepared and used for all microemulsion formulations. A predetermined amount of the AOT surfactant was added to the monomer/cross-linker formulation, and the solution was allowed to stir until all the AOT surfactant was fully dissolved. In order to prepare microemulsions with varying water-to-surfactant ratios, W, a predetermined amount of D_2O was added to the AOT/monomer mixture and stirred vigorously. The photoinitiator was then added to the microemulsion at a concentration of 7×10^{-3} mol/L relative to the monomer volume present. The water-to-surfactant ratio, W, was varied from 5 to 13, and the water content ranged from 5 to 30 mass fraction (%) with respect to monomers. A list of the different microemulsion formulations can be found in Table 1.

Preparation of Films. The films were prepared by placing approximately 2 mL of the microemulsion formulation between two glass microscope slides using glass spacers that were 0.8 mm thick. Samples were photopolymerized with a small hand-held ultraviolet light source (365 nm) with an intensity of 2.3 mW/cm^2 as measured by an International Light (IL1400A) radiometer. The exposure time was 2 min from both sides of the film.

Small-Angle and Ultrasmall-Angle Neutron Scattering (SANS and USANS). The SANS and USANS measurements were carried out on beamlines NG7 and BT5, respectively, at the National Institute of Standards and Technology (NIST) Center for Neutron Research (NCNR), Gaithersburg, MD. The liquid-phase microemulsions were placed in 1.0 mm path length SANS liquid sample holders. Circular shapes were cut out of the films and also placed in 1.0 mm path length SANS sample holders. The NG7 beamline includes a high-resolution 2D detector (65 × 65 cm^2) and focusing refractive lenses. The instrument employs a mechanical velocity selector as a monochromator and a circular pinhole collimator. The SANS intensity, I, was recorded as a function of the magnitude of the scattering vector Q ($Q = 4\pi \sin(\theta/2)/\lambda$, where θ is the scattering angle and λ is the neutron wavelength, equal to 6 Å). The detector angle was set at 0°, and the sample-to-detector distance was set to 1, 4.5, and 13 m to cover the Q-range of 0.003−0.6 Å^{-1}. This setting enables probing structural features in materials ranging from roughly 1 nm to over 500 nm. The USANS measurements were performed

using the BT5 double-crystal diffractometer at the NCNR.[32] Samples were run for 6−8 h each with 1 mm sample thickness in quartz cells. The wavelength of the incident neutrons, λ, was set at 2.38 Å, and data were collected over a Q-range from 2.5×10^{-5} to 5.3×10^{-3} Å^{-1}. For both SANS and USANS, the measured intensity was converted to absolute intensity by correcting for transmission and background scattering. All SANS and USANS data were reduced and modeled using software developed at the NIST Center for Neutron Research.[33]

Definition of Parameters. It is necessary to define several of the parameters that we will use in the data analysis. The first of these parameters, W, is the molar ratio of D_2O to AOT surfactant. In some instances it has been more useful to examine the data using a parameter that we define as $\phi_{w/s}$ which is the ratio of the total volume fraction of the water, ϕ_w, to that of the surfactant, ϕ_s, in the system. Finally, one other parameter that has also been shown to be very useful in discussions of the structure of microemulsions[35] is that of the droplet density, which is given by

$$\phi_d = \frac{(\phi_w + \phi_s)}{(\phi_s + \phi_w + \phi_m)} \quad (1)$$

where ϕ_w, ϕ_s, and ϕ_m are the total volume fraction of water, surfactant, and monomer, respectively, in the microemulsion.

Scattering Theory

Over the past three decades, small-angle neutron scattering (SANS) has proven to be a useful tool in examining the structure of water-in-oil (and oil-in-water) microemulsion systems.[35−42] Although a complete review of the literature is beyond the scope of this paper, it is necessary to discuss a few seminal contributions to this area of research. Studies by Kotlarchyk and co-workers[43−48] used SANS to elucidate the structure in pure three-component AOT/D_2O/alkane systems. Their results have shown that the droplets in such systems are polydisperse spheres and are weakly interacting at room temperature. Furthermore, they showed that the droplet radius increased linearly with an increase in the molar ratio of D_2O to AOT (W = [D_2O]/[AOT]). In particular, they found, empirically, that the mean droplet radius $\langle r \rangle$ could be expressed in terms of W using the following equation:[43]

$$\langle r \rangle = \frac{3v_{D_2O}}{a_o} W + \frac{3V_H}{a_o} \quad (2)$$

Where v_{D_2O} is the volume of a D_2O molecule, V_H is the volume of the "water-penetrated" portion of a single AOT headgroup, and a_o is the area per AOT headgroup on the water−core surface. In related work by Kotlarchyk and co-workers,[45] modeling of the SANS data was accomplished using a form factor for polydisperse hard spheres and structure factors which took into account contributions from interparticle interactions and density fluctuations.

The total scattering function, $I(Q)$, of a microemulsion system can be described by the product of the contributions from the shape of the scattering particle (i.e., the form factor), $F(Q)$, and the spatial distribution of the these scattering particles, or structure factor, $S(Q)$, given by the following relation:

$$I(Q) = n\left|\langle F(Q)\rangle\right|^2 \langle S(Q)\rangle \quad (3)$$

where n is the number density of the scattering particles and the brackets, $\langle\rangle$, represent the ensemble average due to thermal fluctuations. Our present work uses a core−shell model for spherical droplets for $F(Q)$ that considers the core to be polydisperse and the shell to consist of a monolayer of the surfactant molecules. The polydispersity is taken into account by weighting the form factor by a probability function described by the Schulz distribution.[44,45,49] This is a common technique used to describe the polydispersity of droplet size in microemulsions. The form factor, $F(Q)$, for a spherical core−shell particle can be expressed by

$$F(Q) = V_c(\rho_c - \rho_s)\, F_0(QR_c) + V_s(\rho_s - \rho_{solvent})\, F_0(QR_s) \quad (4)$$

where V_c and V_s are the volumes of the particles with radii of the core, R_c, and of the shell, R_s, respectively.[50] Neutron-scattering length densities of the core, shell, and solvent are ρ_c, ρ_s, and $\rho_{solvent}$, respectively. The function $F_0(x)$ is the first-order spherical Bessel function of the first kind and is given by

$$F_0(x) = 3\frac{\sin x - x\cos x}{x^3} \quad (5)$$

The contribution to $I(Q)$ from the structure factor, $S(Q)$, for the spherical core−shell particles has been modeled assuming hard-sphere interactions. This approach has been found to describe scattering from micoremulsions quite well.[9,44] The model structure factor employed here is based on the Percus−Yevick approximation.[51]

Discussion

Microemulsions. Scattering patterns for a series of microemulsions with increasing $\phi_{w/s}$ (between 0.4 and 0.6) are presented in Figure 1. As $\phi_{w/s}$ increases, there is a qualitative change in the scattering behavior. At low $\phi_{w/s}$ (0.44), the microemulsion has a low total volume fraction of water, ϕ_w (0.037), and W is approximately 9.4. Under these conditions, the scattering is most likely due to spherical core−shell droplets that are not correlated with one another; therefore, the scattering represents the form factor described by eq 4. However, as $\phi_{w/s}$ increases, there is an obvious structure peak (maximum) that develops and increases in intensity and shifts to higher Q values with an increase in $\phi_{w/s}$.

(32) Barker, J. G.; Glinka, C. J.; Moyer, J. J.; Kim, M. H.; Drews, A. R.; Agamalian, M. *J. Appl. Crystallogr.* **2005**, *38*, 1004–1011.
(33) Kline, S. R. *J. Appl. Crystallogr.* **2006**, *39*(6), 895–900.
(34) Nagao, M.; Seto, H.; Shibayama, M.; Yamada, N. L. *J. Appl. Crystallogr.* **2003**, *36*, 602–606.
(35) Kotlarchyk, M.; Quirke, N.; Huang, J. S.; Safran, S. A.; Kim, M. W.; Grest, G. S. *Phys. Rev. Lett.* **1984**, *53*(6), 592–595.
(36) Strey, R.; Winkler, J.; Magid, L. *J. Phys. Chem.* **1991**, *95*(19), 7502–7507.
(37) Capuzzi, G.; Pini, F.; Gambi, C. M. C.; Monduzzi, M.; Baglioni, P.; Teixeira, J. *Langmuir* **1997**, *13*, 6927–6930.
(38) Gambi, C. M. C.; Giordano, R.; Laurati, M.; Lanzi, L.; Pini, F.; Baglioni, P. *Appl. Phys. A: Mater. Sci. Process.* **2002**, *74*, S377–S379.
(39) Robinson, B. H.; Heenen, R. K.; Eastoe, J.; Steytler, D. C.; Fragneto, G. *Phys. B* **1992**, *180−181*, 555–557.
(40) Nagao, M.; Seto, H.; Okuhara, D.; Okabayashi, H.; Takeds, T.; Hikosaka, M. *Phys. B* **1998**, *241−243*, 970–972.
(41) Simmons, B.; Irvin, G. C.; Li, S.; John, V.; McPherson, G. L.; Balsara, N.; Agarwal, V.; Bose, A. *Langmuir* **2002**, *18*, 624.
(42) Simmons, B.; Agarwal, V.; McPherson, G. L.; John, V.; Bose, A. *Langmuir* **2002**, *18*, 8345–8349.
(43) Kotlarchyk, M.; Chen, S. H.; Huang, J. S. *J. Phys. Chem.* **1982**, *86*, 3273–3276.
(44) Kotlarchyk, M.; Chen, S. H. *J. Chem. Phys.* **1983**, *79*(5), 2461–2469.
(45) Kotlarchyk, M.; Chen, S. H.; Huang, J. S.; Kim, M. W. *Phys. Rev. A* **1984**, *29*, 2054–2069.
(46) Kotlarchyk, M.; Chen, S. H.; Huang, J. S.; Kim, M. W. *Phys. Rev. Lett.* **1984**, *53*(9), 941–944.
(47) Kotlarchyk, M.; Chen, S. H.; Huang, J. S. *Phys. Rev. A* **1983**, *28*(1), 508–511.
(48) Kotlarchyk, M.; Huang, J. S.; Chen, S. H. *J. Phys. Chem.* **1985**, *89*(20), 4382–4386.
(49) Chen, S. H.; Rouch, J.; Sciortino, F.; Tartaglia, P. *J. Phys.: Condens. Matter* **1994**, *6*, 10855–10883.
(50) Eastoe, J.; Hetherington, K. J.; Sharpe, D.; Dong, J.; Heenen, R. K.; Steytler, D. C. *Colloids Surf., A* **1997**, *128*, 209–215.
(51) Percus, J. K.; Yevick, G. J. *Phys. Rev.* **1958**, *110*, 1.
(52) Caponetti, E.; Chillura-Martino, D.; Ferrante, F.; Pedone, L.; Ruggirello, A.; Liveri, V. T. *Langmuir* **2003**, *19*(12), 4913–4922.

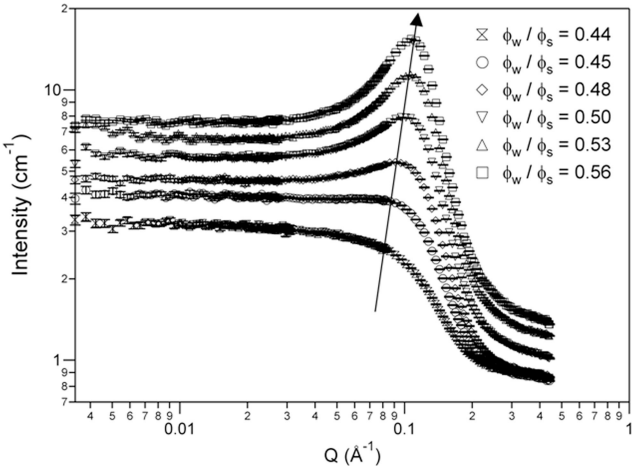

Figure 1. Absolute scattering intensity versus scattering vector, Q, for a set of microemulsions with $\phi_{w/s}$ ranging from 0.4 to 0.6. The scattering curves have been offset vertically for comparison.

This peak is due to interdroplet correlations and will be discussed in greater detail below.

The fitting of the scattering curves was done using a global fitting procedure where the scattering length density of the solvent (monomer), core (D_2O), and shell (AOT) were fixed to values of $\rho_{monomer} = 2.75 \times 10^{-7}$ Å^{-2}, $\rho_{D_2O} = 6.36 \times 10^{-6}$ Å^{-2}, and $\rho_{shell} = 1.78 \times 10^{-7}$ Å^{-2}, respectively. It was assumed that the shell thickness consisted of a monolayer of AOT surfactant[48] and that this shell thickness should be constant among the different microemulsions. The value of the scattering length density was calculated for the surfactant (excluding the sodium sulfonate headgroup) using group parameters found in the literature.[52] It should be noted that several values of ρ_{shell} were systematically chosen to determine which part of the surfactant shell was contributing to the overall scattering intensity. The value given above was found to give the best fits. The fitting parameters for the particle volume fraction, the polydispersity, and the particle radius were left as free parameters to be fit.

Figure 2 shows fitting results for a series of samples containing approximately 10 and 25 mass fraction (%) of D_2O with respect to the monomers and values of W equal to 5, 10, and 13, respectively. As can be seen, the model is in excellent agreement with the experimental scattering data. It should be pointed out that, at lower water contents, the fits are much better over the entire Q-range when compared to the higher water content microemulsions. At higher water contents, the larger droplets may not be spherical. However, the fits are still acceptable, and several other models were systematically investigated; but none represented the data better than the one chosen for this study. The shell thickness that simultaneously fits all the data most appropriately was found to be approximately 5 Å. One would assume that the shell thickness should be comparable to the length of the AOT molecule, which has been reported in the range of 12.9−13.3 Å.[53,54] We propose that the smaller thickness of the surfactant layer can be attributed to low contrast between the surfactant and the monomer phase. In addition, the head of the surfactant is hydrated and its scattering is mixed with the scattering of the D_2O phase. This is consistent with the picture presented by Chen and co-workers.[48] In their model of the

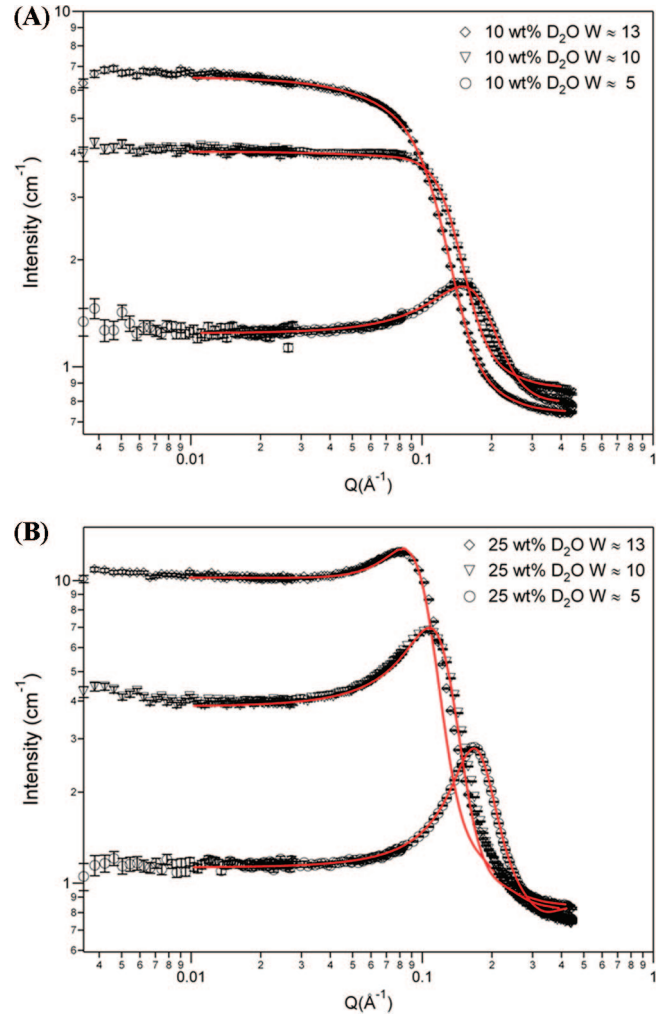

Figure 2. Scattering patterns of two sets of microemulsion: (A) microemulsions with $\phi_w \approx 0.067$ (±0.006) and changing W and (B) microemulsions with $\phi_w \approx 0.14$ (±0.02) and changing W. Lines represent fits of the scattering model to the data.

structure of inverse AOT micelles (Figure 4 of ref 49), they show the tail of the surfactant to be approximately 8 Å in length with the oil phase penetrating the tail by ~2.4 Å, seen also by others.[37,55] Taking this into consideration, it is likely that only about 5 Å of the surfactant in the present systems contributes to the scattering form factor.

We have found that the total droplet core radius is determined by both the total water volume fraction as well as $\phi_{w/s}$. By plotting the total droplet radius (including the shell) as a function of ϕ_w (Figure 3), one can clearly see that there are three regimes governing the growth of the droplet size with increasing water content. By extrapolating the data from the regime II to $\phi_w = 0$, we obtain a value of ~16 Å for the radius of a "dry" droplet, or micelle. Although there are not enough data to do a legitimate extrapolation in regimes I and III, a fit to the two data points in each regime taken together with the fit from regime II yield a value of the dry micelle of 16 ± 1 Å. This is an excellent agreement with values reported in the literature.[48,55,56] It is interesting that the predicted dry micelle radius is considerably larger than the shell thickness chosen to model the data. This shows that the incorporation of the hard-sphere structure factor into our model properly accounts for interparticle interactions. While we have

(53) Simmons, B.; Taylor, C.; Landis, F.; John, V. T.; McPherson, G.; Schwartz, D.; Moore, R. B. *J. Am. Chem. Soc.* **2001**, *123*(10), 2414–2421.
(54) Kotlarchyk, M.; Chen, S.-H.; Huang, J. S.; Kim, M. W. *Phys. Rev. Lett.* **1984**, *53*(9), 941–944.
(55) Maitra, A. *J. Phys. Chem.* **1984**, *88*(21), 5122–5125.
(56) Zulauf, M.; Eicke, H.-F. *J. Phys. Chem.* **1979**, *83*(4), 480–486.
(57) Teubner, M.; Strey, R. *J. Chem. Phys.* **1987**, *87*(5), 3195–3200.

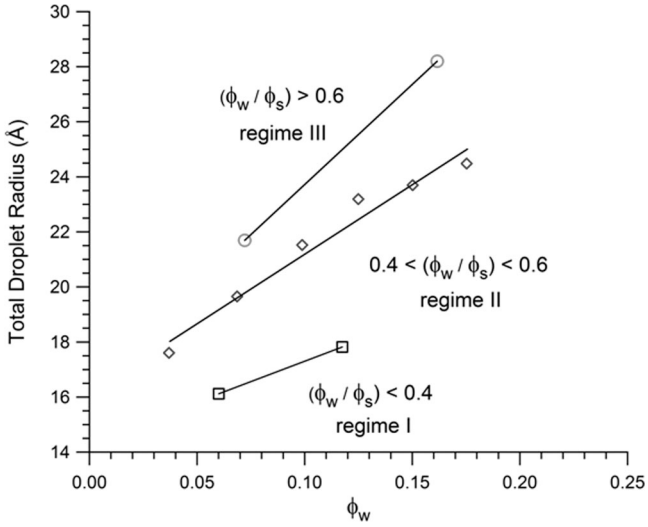

Figure 3. Total droplet radius in Å versus the water volume fraction, ϕ_w, for microemulsions over a range of $\phi_{w/s}$.

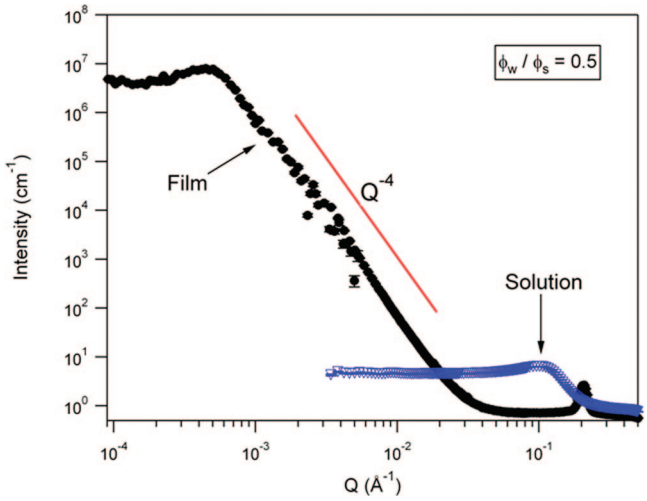

Figure 4. SANS and USANS data showing the structural change upon polymerization of a microemulsion with $\phi_{w/s} = 0.5$.

not taken into consideration the "true" thickness of the AOT monolayer in the form factor, this is compensated for by the chosen hard-sphere structure factor that accounts for how the droplets interact with one another. In other words, the closer that the particles can approach one another, and the smallest radius attainable, is dictated by the total length of the surfactant.

Photopolymerized Microemulsions. Upon photopolymerization of the microemulsions, the optically clear dispersions are transformed into opaque films.[31] This can be explained by a major reorganization of the nanoscale microemulsion structure into structures large enough to scatter visible light. Evidence of this structural change is revealed in the SANS/USANS scattering profiles in Figure 4 for the microemulsion with $\phi_{w/s} = 0.5$. The SANS profile is shown to go from the representative scattering of the microemulsion to a scattering profile of the film which shows a well-defined peak in the high Q-range of 0.15−0.25 Å^{-1} and a scattering feature in the USANS range of 10^{-4}−10^{-3} Å^{-1} which is due to much larger structures. This behavior was observed for all samples, and the position of the high-Q peak and the nature of low-Q scattering are clearly influenced by both ϕ_w and $\phi_{w/s}$.

Figure 5A shows the position of the high-Q peak as a function of $\phi_{w/s}$. In order to relate this peak to a real-space size scale, the

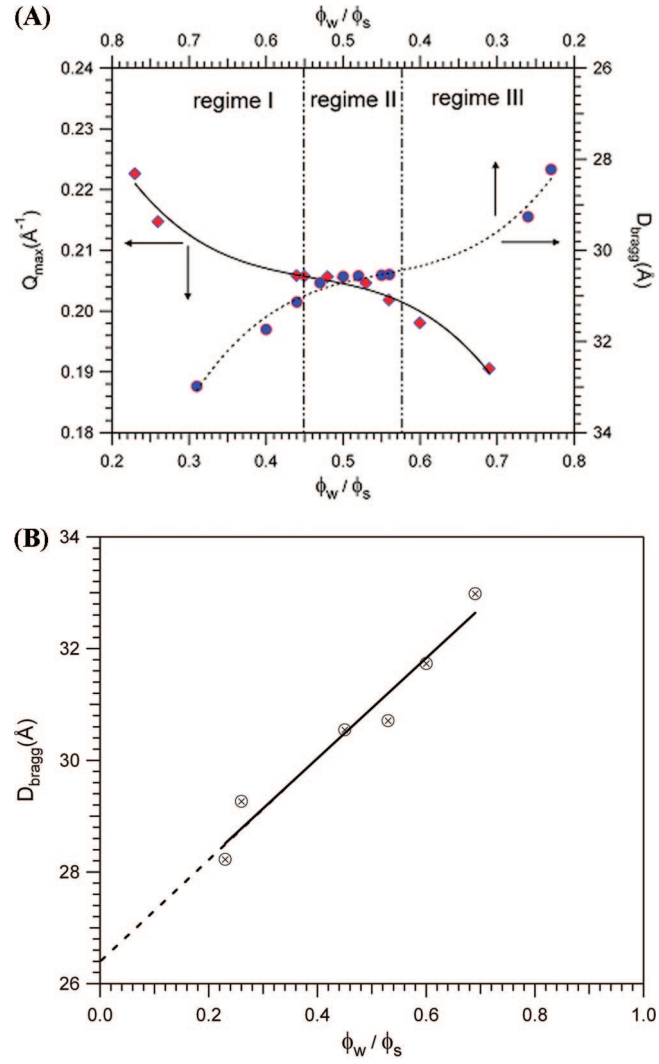

Figure 5. (A) Position in Q (◇) and corresponding D-spacing (○) for the high-Q peak in the polymerized microemulsion films. Lines are present to guide the eye. (B) Corresponding D-spacing for films containing $\phi_w \approx 0.067$ (±0.006) and $\phi_w \approx 0.14$ (±0.02) over a range of W values (i.e., varying $\phi_{w/s}$). The line represents a linear fit to the data and extrapolation to the y-intercept.

D-spacing was calculated from Q_{max} using Bragg's law given by

$$D_{Bragg} = \frac{2\pi}{Q_{max}} \tag{6}$$

and is also plotted in Figure 5A. It is apparent that the position of the high-Q peak, and subsequently D_{Bragg}, is clearly dependent on $\phi_{w/s}$. While D_{Bragg} is continuous as a function of $\phi_{w/s}$, there are three noticeable regimes to the scattering behavior (designated by the vertical, dotted lines). In the range of $0.4 < \phi_{w/s} < 0.6$ (regime II), there is little change in D_{Bragg} associated with the scattering peak. However, above and below this regime, there is strong dependence of D_{Bragg} on $\phi_{w/s}$. In order to gain a deeper insight into the effect of $\phi_{w/s}$ on the structure, we have chosen to plot the data for two sets of samples (Figure 5B), where ϕ_w is held relatively constant ($\phi_w \approx 0.067$ (±0.006) and $\phi_w \approx 0.14$ (±0.02)) while W assumes values of 5, 10, and 13. The D_{Bragg} data from both sets of samples appear to fall on the same line. A linear fit to these data yields an intercept, at $\phi_{w/s} = 0$, of approximately 26 Å. This spacing is equal to roughly twice the reported length of the surfactant molecule. This is verification

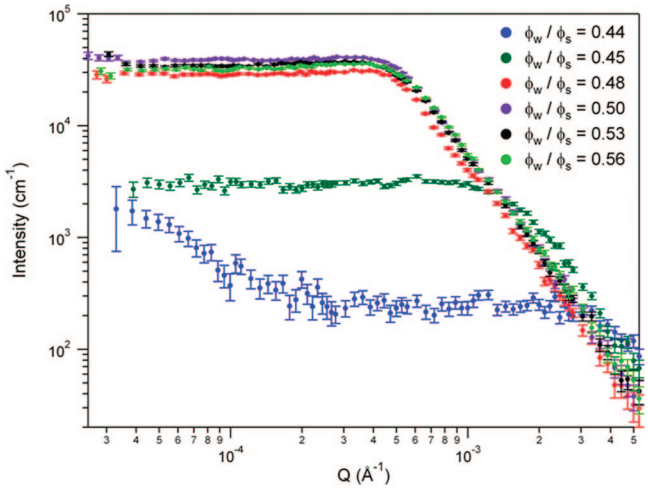

Figure 6. USANS data for films with $\phi_{w/s}$ ranging from 0.4 to 0.6.

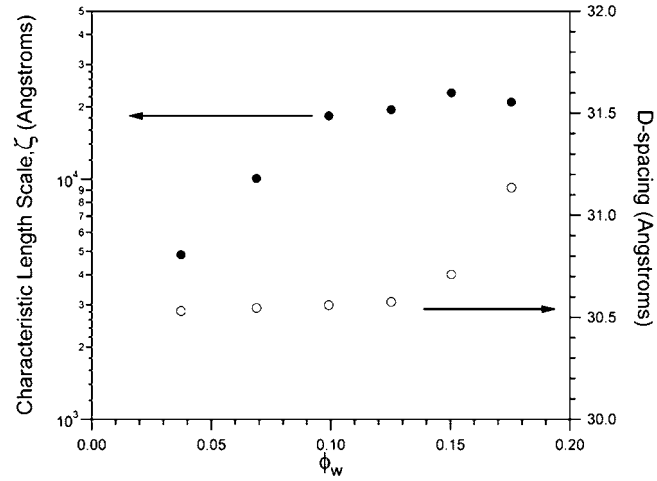

Figure 7. Characteristic length scale, ξ, determined from USANS and the D-spacing associated with high-Q peak versus ϕ_w for films with $\phi_{w/s}$ ranging from 0.4 to 0.6.

that the structure giving rise to the high-Q peak is likely coming from lamellar-like bilayers of the surfactant molecule, in which the bilayers are swollen with water.

Moving along the scattering curve toward lower values of Q, one first finds that in the Q-range from 10^{-3} to 10^{-2} Å^{-1} the scattering follows a Q^{-4} dependence. This is true for all the polymerized microemulsions and indicates that the large structures, or domains, responsible for the low-Q scattering are distinct domains characterized by a sharp interface.[57,58] There is also a structure peak in the range of 2×10^{-4}–7×10^{-4} Å^{-1} indicating a correlation between the large-scale inhomogeneities and finally a leveling off of the scattering intensity at ultralow scattering vectors. The smeared USANS data for the films in the range of $0.4 < \phi_{w/s} < 0.6$ are shown in Figure 6. Above a $\phi_{w/s}$ value of approximately 0.45, there is little change in the scattering behavior. Although it is not discernible in the log−log plot of intensity versus Q, there is a distinct maximum in each scattering curve located in the region just before the scattering follows a Q^{-4} power law dependence. This maximum indicates a structural correlation between the large inhomogeneities giving rise to the ultralow-Q scattering, and the characteristic length scale, ξ, which was calculated from this maximum using Bragg's law.

In order to get a clear picture of the role that water content plays in the development of this structure, we have chosen to plot the ξ data for films prepared from microemulsions in which W remains relatively constant (10.6 ± 1) (this corresponds to $0.4 < \phi_{w/s} < 0.6$). These data, along with the D-spacing for the corresponding high-Q peak in the same films, can be seen in Figure 7. These data show that as the water volume fraction increases, so does the characteristic length scale between the large domains. However, above a value of $\phi_w \approx 0.10$, there is little change in the dimension associated with the correlation distance between the large domains. It is apparent that the D-spacing starts to increase, albeit a small increase, for the bilayer structure. It should be noted that this value of the water content corresponds to a droplet density of ~0.30. This indicates that, above a critical droplet density, the large domains remain relatively unchanged in their structure, while the smaller structures are capable of swelling with water. The implications of these data on the proposed morphology for these systems will be discussed in greater detail.

Several models for the morphology could be chosen to explain the scattering observed for the polymerized microemulsion films. As discussed in our earlier work, it is necessary to discern whether, or not, polymerization simply induced phase separation or if it led to an actual rearrangement of the water and surfactant, thus altering the shape and size distribution of the microemulsion droplets.[31] Moreover, another likely scenario is that phase separation occurs simultaneously with an altering of the nanostructure of the microemulsion droplets. It is known that, by adding polymer to the oil phase in an inverse microemulsion, one can induce phase separation. Xia and co-workers found that, above a critical concentration of the polymer in the oil phase, the microemulsions transition from clear to turbid, indicating phase separation.[59] In the current study, the entire oil phase is polymerizable, making it certain that the polymer concentration is high enough to induce phase separation. Although the results from Xia et al. can explain, in large part, the qualitative observations made in the current system,[31] their experimental results were solely based on turbidity measurements, which do not give any insight into the role that phase separation plays in the self-assembly of the surfactant.

It is apparent that the high-Q peak is indeed due to scattering from a bilayer of the surfactant molecules with water located between the layers. Furthermore, the Q^{-4} power law behavior indicates a sharp interface between the polymer matrix and the large heterogeneities. We propose that, upon polymerization, the change in volume of the monomer mixture into a polymer network causes phase separation via aggregation of the surfactant that stabilized water droplets into larger water droplets. The driving force for this aggregation can be understood by examining the various contributions to the free energy associated with the formation of the microemulsion droplets (ΔG_{form}). The expression for ΔG_{form} is given by

$$\Delta G_{form} = \Delta A \gamma_{1,2} - T\Delta S \qquad (7)$$

where ΔA is the change in the interfacial area between the water and the continuous phase, $\gamma_{1,2}$ is the interfacial tension between the two phases, ΔS is the overall change in entropy of the system, and T is the temperature.[31] As the polymerization occurs, the entropy term is reduced significantly because (1) the number of possible conformations of the droplets is reduced and (2) water

(58) Roe, R.-J. *Methods of X-ray and Neutron Scattering in Polymer Science*; Oxfod University Press: New York, 2000.
(59) Xia, K.-Q.; Zhang, Y.-B.; Tong, P.; Wu, C. *Phys. Rev. E* **1997**, *55*, 5792–5795.
(60) Singh, M.; Tan, G.; Agarwal, V.; Fritz, G.; Maskos, K.; Bose, A.; John, V.; McPherson, G. *Langmuir* **2004**, *20*(18), 7392–7398.

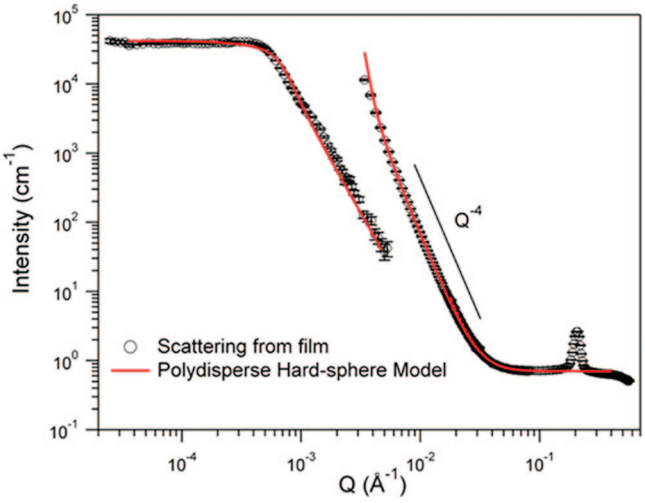

Figure 8. Fit of a polydisperse hard-sphere model to the SANS and USANS scattering data of a polymerized film with $\phi_{w/s} = 0.5$.

can no longer exchange freely between droplets, thus the entropy of mixing decreases. As a result, the overall free energy of the system is increased. The only viable means to lower the free energy is to decrease the total surface area, which is achieved through droplet aggregation. The larger droplets of water are likely stabilized by some fraction of the surfactant, whereas the rest of the surfactant is partitioned to the matrix as bilayer structures swollen with water. In order to determine the plausibility of this explanation, the entire scattering curve for the film ($\phi_{w/s} = 0.5$) was fit with a simple polydisperse spherical droplet model with hard-sphere interactions where the contrast factor was based on the contrast between D_2O and the polymer matrix. The results of this fit to the data can be seen in Figure 8. In Figure 8, the USANS data have not been desmeared and, as result, do not blend seamlessly with the SANS data. However, the data in this form give much more reliable fit results. The USANS and SANS data were fit simultaneously using a model that accounts for instrument smearing of the data. The volume fraction of droplets in the corresponding microemulsion was assumed to be very similar to the droplet density (≈0.38) calculated for this system based on the formulation. With this minor assumption, this model describing the morphology represents the data quite well. Discrepancies can be explained by considering that the model is not very detailed and does not take into consideration (1) the surfactant shell surrounding the larger water droplets, or (2) how much of the water and surfactant are located in the bilayer structures. This explanation is further supported by the data in Figure 7. The characteristic length scale increases until $\phi_w \approx 0.10$ ($\phi_d \approx 0.30$), above which there is little change. The bilayer structures, however, show a different behavior. The *D*-spacing is unchanged until $\phi_w \approx 0.10$, after which there appears to be an increase. This means that the large droplets can only support a certain amount of water, probably dictated by the amount of surfactant in the system, and that the "excess" water is contained in the bilayer structures present in the matrix of the film. Once the larger droplets are "saturated", the bilayers can compensate by swelling with water. Although the exact morphology of the bilayer structures is not known, it is that these structures resemble the self-assembled fibular structures in AOT-based organogels observed by John and co-workers.[53,60] It is also likely that these bilayer structures could contribute to the low-*Q* scattering if they undergo a large degree of aggregation. However, in order to refine our model and to determine the exact nature of the different levels of organization and self-assembly present within these systems, further systematic investigations must be carried out. In particular, the exact origins of the high-*Q* peak can be determined by varying the contrast between the phases. Also, the larger structures observed by USANS can be investigated using phase contrast optical microscopy. While it has been observed that the optical characteristics of these films are dependent upon the humidity,[31] it also follows that a more thorough investigation of the scattering as a function of humidity should be carried out, which should give a better insight into the accuracy of this model and the mechanism for the switching in optical properties of these materials.

Conclusions

SANS and USANS have been employed to investigate the effects of photopolymerization on the structure of inverse microemulsion systems formed from AOT/water/monomer systems. The SANS profiles for the microemulsions were shown to be sensitive to the total amount of water, as well as $\phi_{w/s}$, and were successfully fit with a model for spherical, core−shell droplets with hard-sphere interactions. From this model, the droplet core and shell size were determined for each microemulsion system. These data revealed that the droplet growth, with increasing water content, was highly dependent upon $\phi_{w/s}$. The SANS/USANS profiles of the photopolymerized films reveal that the nanometer size water droplets in the microemulsions rearrange upon polymerization to form two different structures. Large droplet structures are formed from the aggregation of the nanometer size droplets in the microemulsion. These droplets are large enough to scatter visible light and give the films their opacity. Secondly, some portion of the surfactant self-assembles into a bilayer structure characterized by a peak in the high-*Q* range of 0.15−0.25 Å^{-1}. In order to confirm this description, further scattering studies and optical microscopy are needed.

Acknowledgment. The authors would like to acknowledge the financial support provided for these studies from the National Science Foundation Materials Research Science Engineering Center (DMR 0213883) at The University of Southern Mississippi. K.A.P. gratefully acknowledges support from the National Academy of Science, National Research Council Research Associateship Program. Special thanks to Dr. Steve Kline at the NCNR for his input on modeling of the SANS data.

LA8022634